J. Membrane Biol. 184, 61–69 (2001)
DOI: 10.1007/s00232-001-0074-5

The Journal of
Membrane
Biology

© Springer-Verlag New York Inc. 2001

Impact of Apoplast Volume on Ionic Relations in Plant Cells

D. Gradmann
Abteilung Biophysik der Pflanze, Universität Göttingen, Untere Karspüle 2, 37073 Göttingen, Germany

Received: 8 March 2001/Revised: 20 June 2001

Abstract. Ionic relations of plant cells with free-running transmembrane voltage, *V*, can be modelled by electrocoupling of known, *V*-relevant and *V*-gated transporters. For cells in vitro, with constant external substrate concentrations, alternating states of solute uptake and release can be predicted. Here the model is extended to treat cells with limited external substrates, e.g., parenchyma cells in situ with a small external space, the apoplast. This model accounts also for cytoplasmic H^+ buffering and apoplastic buffering of H^+, K^+ and Ca^{2+} by fixed anions. In general, the model converges to thermodynamic equilibrium for K^+ between apoplast and symplast, and to equal steady-state rates of uptake and release for Cl^- and H^+. Oscillations of this model are rare and very sensitive to the volume portion of the apoplast.

Key words: Electrocoupling of ion transporters — Fixed-charges buffer — Kinetic membrane model — Transport oscillations — Voltage gating

Introduction

The transmembrane voltage, *V*, of biological membranes controls the performance of ion transporters (e.g., ion pumps, electrophoretic cotransporters, and channels) in both, thermodynamic and kinetic ways. Thermodynamically control is exerted via the driving force $V\text{-}E_i$, where E_i is the equilibrium voltage of a transporter *i*. Kinetic control, *V*-gating, can also be expected in general, because charged residues will necessarily cause *V*-dependent conformation changes in membrane proteins. In fact, *V*-gating has been verified for virtually all ion transporters that have been investigated with respect to the *V*-dependence of their activity. *V*-gating comprises not only the *V*-dependence of the steady-state activity of the transporter but also the velocity by which the activity changes upon a change in *V*. Both characteristics of specific transporters are typically investigated by *V*-clamp experiments, when time courses of electrical currents are recorded upon a *V*-protocol as defined by the experimenter. Major ion transporters can pass enough current to cause significant *V* changes, and have a *V*-dependent activity. Therefore, they are coupled to each other via the free-running *V:* If one major transporter changes its activity, *V* will change, which, in turn, will cause all *V*-gated enzymes (the major transporters included) to change their activity, and so on.

This temporal behavior of an ensemble of major ion transporters can be calculated with the particular thermodynamic and kinetic features of the individual transporters as known from *V*-clamp studies. For plant cells, such *V*-mediated interactions amongst the major ion transporters have already been studied by an initial approach (Gradmann, Blatt & Thiel, 1993) and by a more realistic treatment (Gradmann & Hoffstadt, 1998).

Briefly, Fig. 1*A* illustrates five major ion transporters in the plasmalemma of a plant cell, which represent uptake and release of cations and anions in a crude but consistent approximation: A K^+ outward rectifier, *Ko*, for cation release; a K^+ inward rectifier, *Ki*, for cation uptake; an electrogenic H^+ pump, *Pu*, for energizing; a $2H^+$-Cl^- symporter, *Sy*, for anion uptake, and a Cl^- conductance, *Cl*, for anion release.

Initially (Gradmann et al., 1993), constant equilibrium voltages, E_i, and linear steady-state current-voltage relationships of the active states $I_a(V)$ have been assigned to all five transporters. The main result was that this system alternates between salt (K^+ and Cl^-) uptake and salt release. In this model *A*, the parameters had to be chosen to balance the long-term ionic relations (E_i = *const*).

In the second approach (Gradmann & Hoffstadt 1998), E_i was allowed to change due to uptake and/or release of substantial amounts of K^+ and Cl^-, and the concentration-dependent, nonlinear shape of $I_a(V)$ of the

Correspondence to: D. Gradmann; email: dgradma@gwdg.de

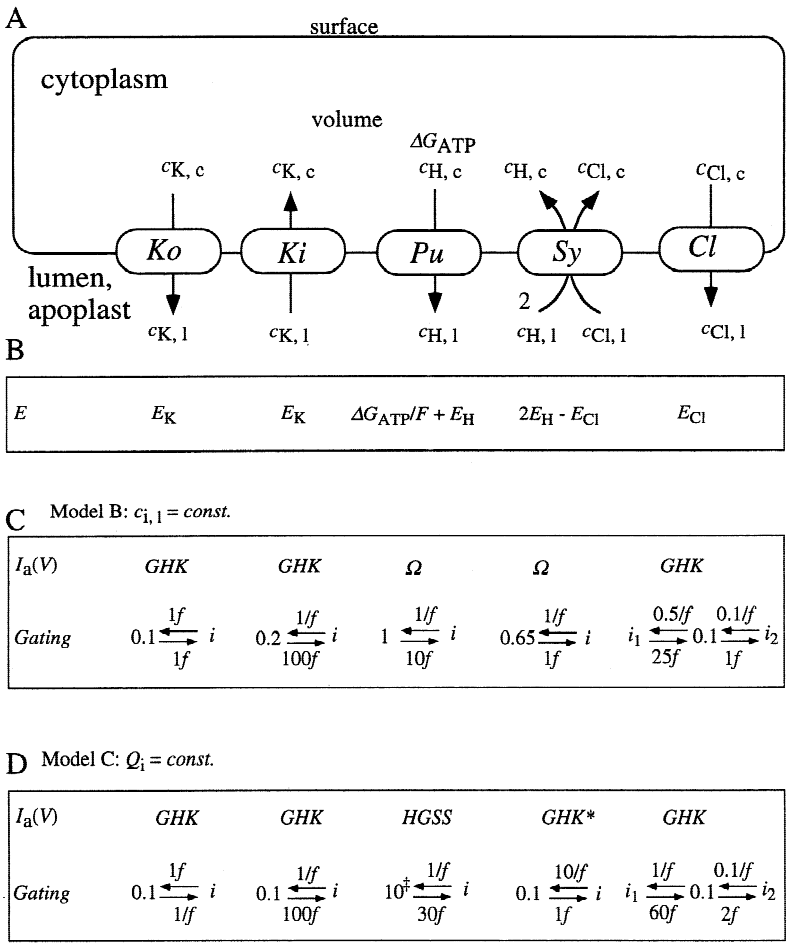

Fig. 1. Synopsis of plasmalemma models with five major ion transporters. Definitions and general arrangement in arbitrary order, from left to right: *Ko*, K^+ outward conductance for release of cations; *Ki*, K^+ inward conductance for uptake of cations; *Pu*, pump (H^+-exporting ATPase) for energizing of ion uptake; *Sy*, symporter ($2H^+$-Cl^-) for uptake of anions, *Cl*, Cl^- conductance for release of anions. (*A*) Schematic arrangement in cell with defined surface/volume ratio; $c_{i,c}$ and $c_{i,l}$: concentrations of transported substrates *i* in cytoplasmic and luminal (apoplastic) compartment, respectively; $\Delta G_{ATP} = F \cdot (-450\ mV)$: free energy of ATP hydrolysis. (*B*) Thermodynamic characterization: equilibrium voltages *E* (reversal voltages, $V_{I=0}$) of the five transporters according to Eqs. *3–5*. (*C*) Kinetic characterization of model *B* ($c_{il} = const.$; here, $c_{K,l} = c_{Cl,l} = 1$ mM; $pH_l = 6$; $pH_c = 7.4$); surface/volume: $10^6\ m^{-1}$, $I_a(V)$, steady-state current-voltage relationships of the five transporters in active states; *GHK*, Eq. *5;* Ω, Eq. *4; Gating:* numbers on head or tail of arrows, maximum conductance; *g* in $Sm^{-2}\ mM^{-1}$ or Sm^{-2} if $I_a(V) = \Omega$; *i:* inactive state with $g = 0$; numbers on arrows, rate constants in sec^{-1}; $f = e^{w/2}$; $u = VF/(RT)$. (*D*) Kinetic characterization of model *C* ($Q_i = const.$): here, start concentrations (total) in mM: 200 A_c, 200 F_l, 200 K_c, 250 K_l, 16 H_c, 50 H_l, 18 Ca_l; dissociation constants, K_D in μM: 1 AH, 1 FH, 100 FK, 1000 F_2Ca; geometry: $10^{-16}\ m^3 = 0.1$ pl volume; $10^{-10}\ m^2$ surface area; $I_a(V)$: as in panel *C*, except *HGSS* = Eq. *6* and *GHK** = Eq. *7; Gating:* symbols as in panel *C*, except ‡ marks not conductance but saturation currents, $\pm I_{pu,mx}$ in $Am^{-2}\mu M^{-1}$, for large $\pm\Delta V$ from E_{Pu} at $c_{H,c} = c_{H,l} = 1$ μM.

active (open) channels has been accounted for by the constant field current equation. In this model *B*, the luminal concentrations, $c_{K,l}$ and $c_{Cl,l}$, of K^+ and Cl^- have been assumed to be constant ($c_{i,l} = const.$). This system converges from various start conditions of cytoplasmic K^+ and Cl^- concentrations, $c_{K,c}$ and $c_{Cl,c}$, towards stable oscillations within narrow ranges of $c_{K,c}$ and $c_{Cl,c}$. In other words, model *B* provides homeostatic osmoregulation without special sensors, such as stretch-activated channels, and without special messengers, such as G-proteins or cytoplasmic Ca^{2+}. The model parameters of the example calculation for Fig. 5 in Gradmann & Hoffstadt (1998) are given in Fig. 1*C* for reference purposes.

The conditions of model *B*, $c_l = const.$, apply to algal cells in situ, which usually have an external compartment of virtually infinite volume, and in general to all single cells in vitro with well-defined bath media.

As for cells of vascular plants in situ, it may partially apply to epidermal cells of roots, especially root hairs, but certainly not for parenchyma cells, which typically have large symplastic and small apoplastic volume. In these cells, the movement of a substrate through the plasmalemma will cause a relatively small concentration change in the large symplast and a much larger concentration change (of the opposite sign) in the small apoplastic volume. Since this situation does not correspond to normal experimental conditions, very little is known about the ionic relations of parenchyma cells in situ.

The aim of this study is to explore the interactive behavior of the five major ion transporters in parenchyma cells, i.e., cells with a small portion of apoplastic volume. The limiting assumption of this model *C* is constancy of the total quantities ($Q_i = const.$) of the various ionic substrates, which are redistributed in varying portions between symplast and apoplast.

For a realistic treatment of this model *C*, we have to consider buffering of cations by a substantial concentration of fixed negative charges, F^-, in the apoplast: When a certain amount of, let's say, H^+ leaves the cell, only a portion of it will increase the concentration of free H^+ in the apoplast, another portion will associate with F^- and release certain quantities of other cations from their association with F^-, with the effect that also the concentrations of the other free cations will increase. Fig. 2

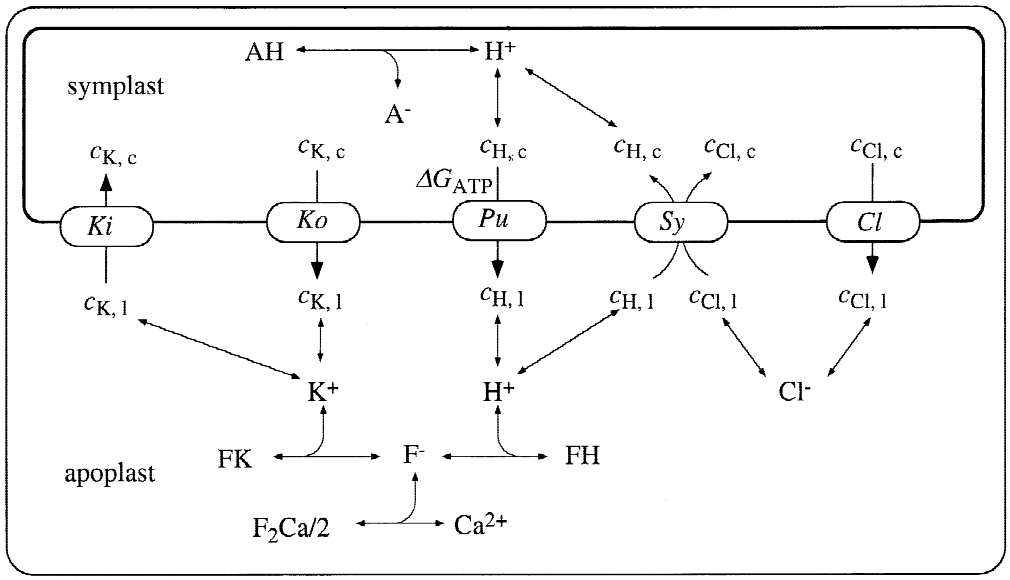

Fig. 2. Model of ionic relations of a parenchyma cell. Small apoplastic volume with considerable concentration of fixed charges F^- which can bind the transportees K^+ and H^+ and the nontransported Ca^{2+} in the apoplast; large symplastic volume with H^+ buffer *A*. For quantitative aspects, *see* Eqs. *8*, *10*, *11* and *12*.

illustrates these relationships, as well as corresponding internal H^+ buffering, which are accounted for by model *C*.

The present version *C* of the model does not account for many processes that affect the electrical behavior of plant membranes as well. In particular, ligand gating e.g., of the K^+ conductance by external K^+ (Beilby & Blatt 1986), or of the Cl^- conductance by cytoplasmic Ca^{2+} (Biskup, Gradmann & Thiel, 1999), and known effects of pH on the H^+ pump (Blatt, 1987; Blatt, Beilby & Tester, 1990). Implementation of such processes is possible but beyond the scope of the present study, which focuses on the apoplast.

In a wider context, a precursor version of model *C* has already been presented at a meeting (Gradmann 2001).

Theory

Fig. 1*A* illustrates the plasmalemma of a plant cell with five major ion transporters and the relevant concentrations, $c_{i,c}$ and $c_{i,l}$ of the ions, *i*, on the cytoplasmic and luminal side respectively.

Thermodynamic Relations

Fig. 1*B* lists the thermodynamic characteristics in form of the equilibrium voltages, E_i, at which the driving forces of the particular transport (concentration gradients, *V*, and metabolic energy input in case of *Pu*) add up to zero. For the uniporters *Ko*, *Ki*, and *Cl*, it is the Nernst equilibrium voltage

$$E_i = \frac{-RT}{z_i F} \ln \frac{c_{i,c}}{c_{i,l}} \tag{1}$$

for an ion *i* with the charge number z_i, where *F*, *R*, and *T* have their usual thermodynamic meanings.

E_{Pu} of an electrogenic pump that translocates *n* H^+ per ATP is

$$E_{Pu} = \frac{\Delta G_{ATP}}{nF} + E_H \tag{2}$$

where $\Delta G_{ATP}/F$ is assumed here to be −450 mV and $n = 1$.

For *Sy* as used here, the explicit equation for the equilibrium voltage of symporters (*not shown here*) assumes the simplified form:

$$E_{Sy} = 2E_H - E_{Cl^-} \tag{3}$$

Kinetic Relations

The kinetic properties assumed for the example calculations with model *B* and model *C* are listed in the boxes Fig. 1*C* and 1*D*. For the steady-state current-voltage relationships $I_a(V)$ of the active transporters, the following relationships have been used: 'Ω' as listed in Fig. 1 *C*, for *Pu* and *Sy*, stands for a linear relationship

$$I_a(V) = g_\Omega (V - E), \tag{4}$$

with a constant, ohmic conductance, g_Ω.

In model *B*, $I_a(V)$ of the uniporters *Ko*, *Ki*, and *Cl* have already been described by the Goldman-Hodgkin-Katz current equation, *GHK*, in the form,

$$I_{GHK}(V) = V g_{GHK} \frac{c_c - c_l e^{-zu}}{1 - e^{-zu}} \tag{5}$$

where g_{GHK} is the reference conductance at 1 mM concentrations on

both sides, and $u = VF/(RT)$ is the normalized membrane voltage. This Eq. (5) is used here in model *C* as well for $I_a(V)$ of *Ko, Ki,* and *Cl.*

For $I_a(V)$ of *Pu,* Eq. (6) is used here

$$I_{Pu}(V) = I_{Pu,mx} \frac{c_{H,c} - c_{H,l} \cdot \exp(u_{ATP} - u)}{1 + \exp(u_{ATP} - u)}, \quad (6)$$

where $I_{pu,mx}$ is the amount of the saturation currents at large *V* displacements, $\pm\Delta V$, from E_{Pu} at $c_{H,c} = c_{H,l} = 1$ μM, and $u_{ATP} = \Delta G_{ATP}/(RT)$. This Eq. *6* is directly derived from the general equation of the current-voltage relationships of active transport (Hansen et al., 1981) with the simplifying assumption that the saturation currents, $\pm I_{Pu,\,mx}$, are symmetrical. The second simplifying assumption ($\kappa_{io}\kappa_{oi} >> \kappa_{io}\kappa_{oi}$, in the nomenclature of Hansen et al. (1981) means that $I_{Pu}(V)$ reaches $\pm I_{pu,mx}$ as fast as possible with $\pm\Delta V$. For reference purposes, e.g., in Fig. 1, Eq. *6* is called *HGSS* according to the authors (*H*ansen, *G*radmann, *S*anders, and *S*layman) in Hansen et al. (1981).

For $I_a(V)$ of *Sy* we used a constant-field formalism, *GHK**, in analogy to Eq. *5*

$$I_{Sy}(V) = Vg_{Sy} \frac{(c_{H,c})^2\, c_{Cl,c} - (c_{H,l})^2\, c_{Cl,l} e^{-u}}{1 + e^{-u}} \quad (7)$$

If saturation of $I_{Sy}(V)$ should be accounted for, the hybrid form

$$I_{Sy}(V)' = I_{Sy,mx} \frac{(c_{H,c})^2\, c_{Cl,c} - (c_{H,l})^2\, c_{Cl,l} e^{-u}}{1 + e^{-u}} \quad (8)$$

between Eq. *6* and Eq. *7* may be applied alternatively.

Gating Relations

The second row *Gating* in the boxes of Fig. 1*C* and 1*D* provides the numerical assumptions for time- and *V*- dependencies of activation/inactivation of each transporter, as used for the example calculations presented here. For every transporter one active state, *a,* and one inactive state, *i,* has been assumed, except for *Cl* which has two inactive states, i_1 and i_2, with *a* in between. In the *Gating* rows of Fig. 1, the numbers at the heads and tails of the arrows mark the reference conductances (in $S \cdot m^{-2}$, at symmetrical 1 mM substrate concentrations) of the active states; only for *Pu,* it marks the saturation currents $\pm I_{Pu,\,mx}$. The numbers along the arrows mark transition probabilities, *k* in sec^{-1}, for activation (k_a) and inactivation (k_i) at $V = 0$. The voltage sensitivities of the *k*'s are expressed by $f = e^{u/2}$ or $1/f = e^{-u/2}$, where the factor 1/2 in the exponents stands for the assumption of a symmetrical energy barrier. With these parameters, the temporal and *V*-dependent characteristics of the activities of the transporters have been calculated by iterative integration of ordinary differential equations with small time increments Δt (for details *see* Gradmann & Hoffstadt, 1998).

Buffer Systems

Fig. 2 illustrates the reactions of the buffer system which has been used to calculate the ionic relations of a parenchyma cell with the five major transporters. In the symplast, all cytoplasmic K^+ and Cl^- is assumed to be free, and H^+ is assumed to be buffered by a virtual anion, A^-, which represents organic anions and acidic compartments. The apoplast is assumed to have a considerable concentration of fixed anions, F^-, which can be free or occupied by Ca^{2+}, H^+, or K^+. Here the complex, apoplastic buffer system is treated in analogy to a Ca^{2+} buffer with competing ligands (Amtmann, Klieber & Gradmann, 1993).

For the buffer calculations, the following relationships of mass conservation have been used:

$$c_{Atot} = c_{A^-} + c_{AH} \quad (8a)$$
$$c_{Ftot} = c_{FK} + 1/2c_{F2Ca} + c_{FH} + c_{F^-}; \quad (8b)$$
$$Q_H = (c_{H,c} + c_{AH})vol_c + (c_{H,l} + c_{FH})vol_l; \quad (8c)$$
$$Q_K = (c_{K,c} + c_{AK})vol_c + (c_{K,l} + c_{FK})vol_l; \quad (8d)$$
$$Q_{Ca} = (c_{Ca} + c_{F2Ca})vol_l; \quad (8e)$$

where vol_l and vol_c are the volumes of the apoplast and protoplast respectively, and Q_H, Q_K and Q_{Ca} denote quantities of H^+, K^+ and Ca^{2+} respectively.

Electroneutrality dictates the Cl^- concentrations:

$$c_{Cl,c} = c_{H,c} + c_{K,c} - c_{A^-} \text{ and} \quad (9a)$$
$$c_{Cl,l} = c_{H,l} + 2c_{Ca} + c_{K,l} - c_{F^-}, \quad (9b)$$

which, again, have to satisfy mass conservation by

$$Q_{Cl} = c_{Cl,c}vol_c + c_{Cl,l}vol_l. \quad (8f)$$

Dissociation constants of the apoplastic F^- buffer are

$$K_{D,FH} = c_{H,l} \cdot c_{F^-}/c_{FH}, \quad (10a)$$
$$K_{D,FK} = c_{K,l} \cdot c_{F^-}/c_{FK}, \quad (10b)$$
$$K_{D,F2Ca} = c_{Ca} \cdot c_{F^-} \cdot c_{F^-}/c_{F2Ca}, \quad (10c)$$

and of the symplastic H^+ buffer

$$K_{D,AH} = c_{H,c} \cdot c_{A^-}/c_{AH}. \quad (10d)$$

With known K_D values and start concentrations of total *A*, H_c, *F*, H_l, K_l, and Ca_l, the initial concentrations of all reactants can be calculated. Key relationships for these calculations are:

$$c_{A^-} = \frac{c_{Atot}}{1 + c_{H,c,tot}/K_{D,AH}}, \text{ and} \quad (11)$$

$$c_{F,tot} = c_{F^-}\left(1 + \frac{c_{H,l,tot}}{c_{F^-} + K_{D,FH}} + \frac{c_{K,l,tot}}{c_{F^-} + K_{D,FK}} + \frac{c_F - c_{Ca,tot}}{c_{F^-}c_{F^-} + K_{D,F2Ca}}\right), \quad (12)$$

which can be obtained by rearranging Eqs. *8* and *10*. Eqs. *11* and *12* provide the essential values of c_{A^-} and c_{F^-} either directly by Eq. *11* or with iterative determination by Eq. *12*.

An initial, cytoplasmic K^+ concentration, $c_{K,\,c}$, has been assumed as well, which does not enter the internal buffer system at time zero; and the initial Cl^- concentrations $c_{Cl,c}$, and $c_{Cl,l}$, are given then by Eqs. *9*.

When the concentrations of all ionic substrates are known, Eqs. *5, 6* and *7* yield the currents at a given *V*. The free-running *V,* i.e., *V* where the sum of all currents in the Table, *C* is zero, has been determined iteratively by Eqs. *5, 6* and *7*. At this *V,* Eqs. *5, 6* and *7* provide the amounts of translocated H^+, K^+ and Cl^- within a small time interval Δt. This results in a redistribution of the cytoplasmic and luminal portions of the total quantities of H, K, and Cl. With the new values of total substrate concentrations, the buffer calculations for cytoplasmic *A* and apoplastic *F*, using Eqs. *11* and *12,* yield updated values for the concentrations of the free ionic substrates. These are used again to calculate a new *V,* and so on.

Software

The program for calculations and display is written in Turbo Pascal, and runs on a PC. The software is free and available on request.

Results

Algorithm

Based on the success of the algorithm of model B (Fig. 1*A–C*) to describe the ionic relations of plant cells with $c_{i,l} = const.$ (Gradmann & Hoffstadt 1998), an attempt was made initially to apply this algorithm to the conditions $Q_i = const.$ However, these attempts with a precursor version of model *C* using Eq. *4* for $I_a(V)$ of *Pu* and *Sy* failed frequently, because of fatal occurrences of $c_i < 0$ during the calculations. Especially $c_{i,l}$ has been critical, because given transport rates cause large changes of $c_{i,l}$ in a small, apoplastic volume. This problem has been eliminated by implementation of Eqs. *6* and *7* into the algorithm. In case of depletion of some substrate, these relationships—like *GHK*—cause the corresponding transport rates to become small. In a preceding report (Gradmann, 2001), an intermediate version of model *C* has been presented, in which Eq. *7* was already used for $I_a(V)$ of *Sy*, but $I_a(V)$ of *Pu* was still calculated with Eq. *4*. There are significant but not fundamental differences between the successful runs of that previous version of model *C* and the actual version presented here.

Oscillations

As a general result, it is much more difficult to find parameter configurations of model *C* (small apoplast) that yield oscillations, than it is with model *B* (infinite bath). Nevertheless, sets of parameters do exist that cause model *C* to generate oscillations. So far, these sets have been found by trial and error, because a systematic analysis of the behavior of model *C* is not available yet. Results from such a successful parameter configuration are illustrated in Figs. 3–5.

Figure 3 demonstrates that the main physiological difference between model *B* and model *C*, namely, the volume of the apoplastic compartment, plays a key role for the ability of model *C* to generate oscillations. Fig. 3*A* shows that with only 9% apoplastic volume, oscillations are completely absent, and *V* relaxes to a rather negative steady-state value. In contrast, with 10% (Fig. 3*B*), complex oscillations are generated, which are reminiscent of the oscillations of model *B* (Gradmann & Hoffstadt 1998), and which consist of a superposition of fast electrical and slow osmotic oscillations. With 12% apoplastic volume (Fig. 3*C*), the fast component of the oscillations becomes predominant, and with 14% apoplastic volume (Fig. 3*D*), these fast oscillations damp out towards a steady-state *V*, which is much more positive than that in Fig. 3*A*.

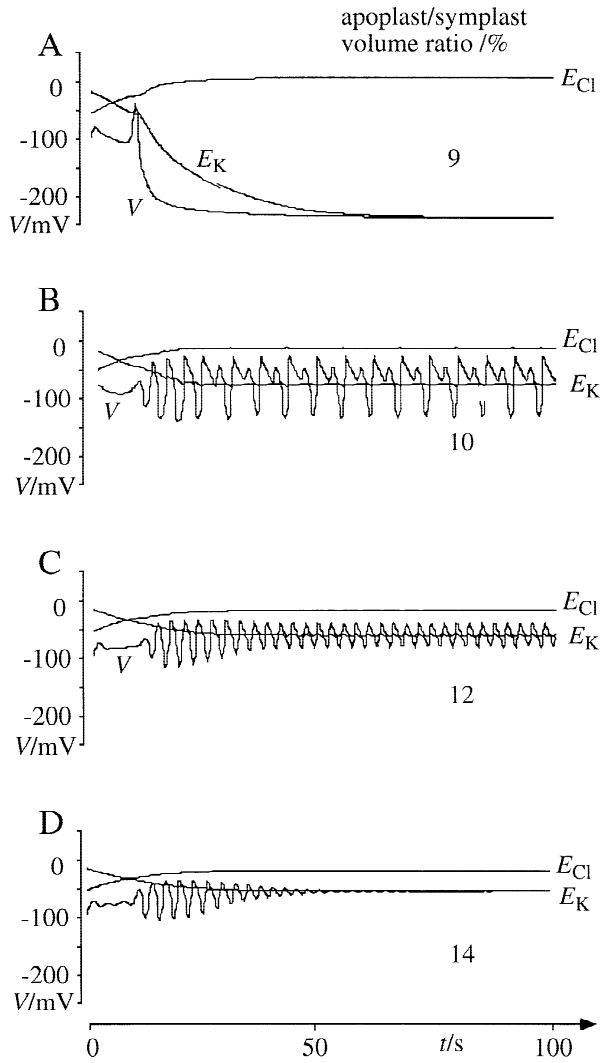

Fig. 3. Effect of apoplast volume on oscillations in model *C* for parenchymatic cells. Small apoplast with fixed charges and large symplast with H^+ buffer; parameters listed in Fig. 1*D*, with given configuration. (*A*) Rapid approach of equilibrium ($V = E_{Pu}$) with small apoplast/symplast volume ratio (≤9%). (*B*) and (*C*): Continuous oscillations occur only in narrow range of apoplast/symplast volume ratio. (*B*) Complex, very nonlinear shape. (*C*) Simple, near sinusoidal shape. (*D*) Slow approach of steady state after damped oscillations with large apoplast/symplast volume ratio (≥14%).

The records of E_K and E_{Cl}, which are plotted in Fig. 3 to the same scale as *V*, reflect the time courses of the distribution of free K^+ and Cl^- between the symplastic and apoplastic compartment. We notice in all traces of Fig. 3 that E_K follows *V* accurately, only with some lowpass delay.

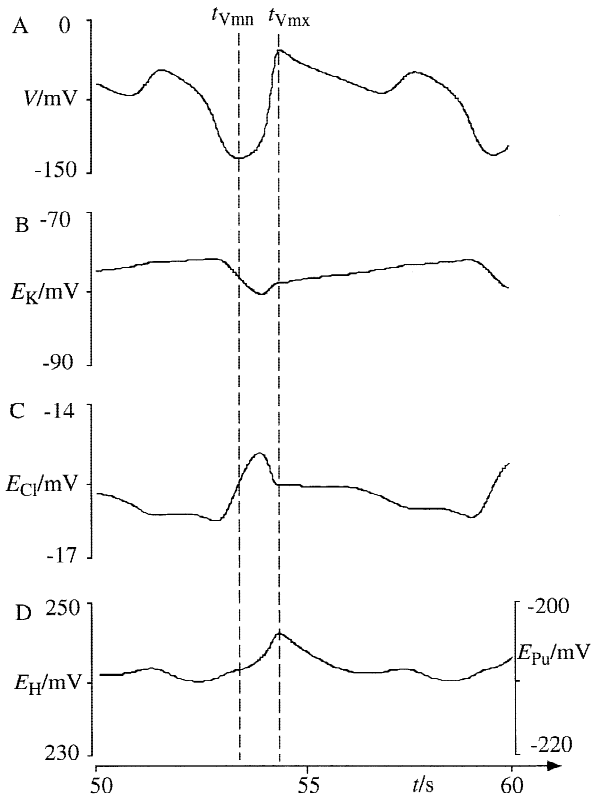

Fig. 4. Oscillations in V and E_i of model *C* with 10% apoplast. Details of behavior of model *C* with parameters listed in Fig. 1 and an apoplast/symplast volume ratio of 10%, between time 50 sec and 60 sec of record shown in Fig. 3*B;* vertical dashed lines mark times of minimum and maximum *V*.

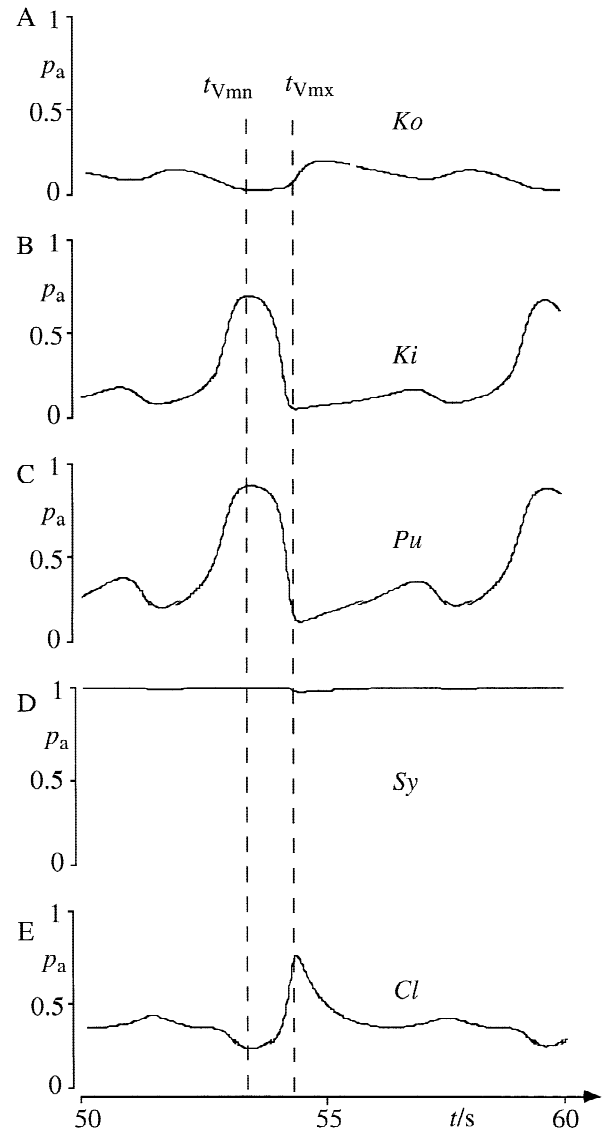

Fig. 5. Oscillations in p_a of the five transporters in model *C* with 10% apoplast. Details of changes in ion p_a of the five transporters during continuous oscillations of model *C*, with parameters listed in Fig. 1 and an apoplast/symplast volume ratio of 10%, between 50 sec and 60 sec of record shown in Fig, 3*B;* vertical, dashed lines mark times of minimum and maximum p_a.

Phase Relationships

The stationary oscillations of model *C* with the parameter configuration of Fig. 3*B* are plotted with better resolution in Figs. 4 and 5. Fig. 4 shows the records of V and E_i including E_H with individual ordinate scales. The dashed, vertical lines are time markers for the minimum and maximum of $V(t)$, t_{Vmn} and t_{Vmx}, in Fig. 4. We notice that during periods of more negative V, E_K becomes more negative and E_{Cl} more positive, which means in terms of Eq. *1* a shift of K^+ and Cl^- from the apoplast to the symplast. The antiparallel time course of E_K and E_{Cl} can be seen throughout Fig. 4*B* and *C*. $E_H = E_{Pu}$ + (450 mV = $-\Delta G_{ATP}/F$) is rather positive and peaks about simultaneously with V_{mx}.

The time courses of the activities of the five transporters in Fig. 5 show that *Sy* was about always at its maximum activity during these oscillations, and *Ko*, in contrast, was rather low ($\leq$0.2) throughout. This result does not mean that these features were essential for the oscillations; other parameter configurations of the model with much higher $p_a(Ko)$ and much lower $p_a(Sy)$ did show oscillations (*results not shown*). The small changes of the $p_a(Ko)$ and $p_a(Sy)$ in Fig. 5 rather suggest that *Ki* and *Sy* play only a minor role for the oscillations shown. In contrast $p_a(Pu)$, $p_a(Ki)$, and $p_a(Cl)$ change considerably during these oscillations.

Using the time markers, we notice that at t_{Vmn} the hyperpolarizing factor $p_a(Pu)$ is in a maximum and the depolarizing factor $p_a(Cl)$, in a minimum and *vice versa* for t_{Vmx}. The time course of $p_a(Ki)$ is parallel to that of $p_a(Pu)$ and antiparallel to $p_a(Ko)$. These results are not surprising as they basically reflect the V-dependences of the transporters as defined in Fig. 1. Nevertheless, these

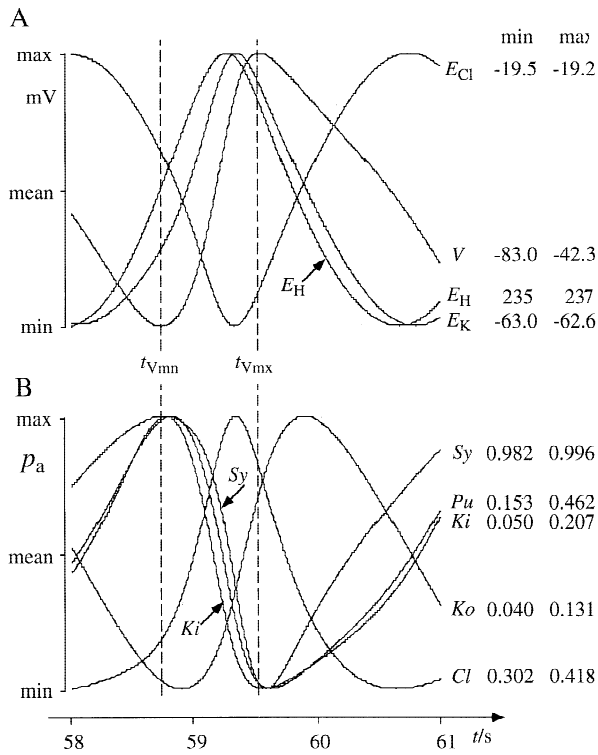

Fig. 6. Phase relationships of oscillations in model *C* with 12% apoplast. Details of changes in the five transporters during continuous oscillations of model *C* with parameters listed in Fig. 1 and 12% apoplast/symplast volume ratio, between 58 and 61 sec of record in Fig. 3*C;* records normalized to maxima and minima as listed in columns on the right hand side; labeled arrows in panels prevent ambiguous assignment of records to transporters. (*A*) relative activities p_a. (*B*) V and E_i; vertical, dashed lines mark time of maximum and minimum of V.

Table. Steady-state properties of model *C* with parameters in Fig. 1.

	Observable steady-state parameter	Apoplast/symplast volume ratio	
		9%	14%
Voltage	V (mV)	−242	−58
Transporter activities, p_a	*Ko*	<0.001	0.094
	Ki	0.993	0.088
	Pu	0.998	0.244
	Sy	0.9999	0.990
	Cl	0.004	0.310
Concentr. of free ions			
	$c_{K,\,c}$ (mM)	222	220
	$c_{K,\,l}$ (mM)	0.02	23
	$c_{H,\,c}$ (μM)	0.022	0.034
	$c_{H,\,l}$ (μM)	76	330
	$c_{Cl,\,c}$ (mM)	27	27
	$c_{Cl,\,l}$ (mM)	20	60
	$c_{Ca,\,l}$ (mM)	3	18
Transporter currents (mAm^{-2})			
	I_{Ko}	<0.001	<0.05
	I_{Ki}	<0.001	<0.05
	I_{Pu}	5.68	83.4
	I_{Sy}	−2.85	−41.7
	I_{Cl}	−2.83	−41.7

results show that the outline and the details of the program are not biased by severe errors.

Since in model *B* fast and slow oscillations could be distinguished by changing the surface/volume ratio (Gradmann & Hoffstadt, 1998), the same strategy has been applied to the complex oscillations of model *C* at 10% apoplast/symplast volume ratio. However, decreasing the surface area in the model by factor 5 causes $V(t)$ to slow down only by about 30% without a substantial change in shape (*result not illustrated*).

The temporal analysis of Fig. 3*B* by Figs. 4 and 5 is rather approximate, first, because the time courses are complex and second, because of the low resolution. A more detailed analysis of the simpler oscillations of Fig. 3*C* is given by Fig. 6. In this diagram we notice considerable phase differences between the individual records. Fig. 6*A* shows that the minima of the cationic E_H and E_K precede t_{Vmn} by about 1.0 and 0.8 sec respectively. The corresponding phase differences to t_{Vmx} are about 0.3 and 0.2 sec. The anionic E_{Cl} fits in this pattern with the opposite sign. The minimum and the maximum of E_{Cl} precede t_{Vmx} and t_{Vmn} by about 0.25 sec and 0.9 sec respectively. In contrast, Fig. 5*B* shows that the time courses $p_a(t)$ of *Pu*, *Ki* and *Sy* lag behind $V(t)$ by about 40–80 ms. This behavior reflects delayed activation of these three transporters by negative V (Fig. 1). Correspondingly, $p_a(t)$ of *Ko* peaks after t_{Vmx} because p_a of *Ko* increases with positive V. Critical, however, is the behavior of the depolarizing transporter *Cl*. Its peak of activity precedes t_{Vmx} by about 0.15 sec.

Steady State

Since oscillations of model *C* are relatively rare (Fig. 3), its steady-state properties are expected to be of more general interest for the ionic relations of parenchyma cells in situ. Steady-state characteristics of two different states of model *C* with the parameters in Fig. 1*B* and *D* can be obtained from the calculations to Fig. 3*A* and *D* at the ends of the records.

The results in the Table show the values of some observable parameters for the two different apoplast/symplast volume ratios (9 and 14%) tested. As already shown in Fig. 3, the steady-state V for 9% is much more negative than for 14%. In fact, the system converges to $V = E_{Pu}$ at 9%, and the degenerated steady-state activi-

ties $p_a = 1/(1 + k_i/k_a)$ of all transporters reflect the small numerical value of $f \approx 0.01$ at $V \approx -240$ mV. For the steady state at 14% apoplast volume, the p_a values assume intermediate values between 0 and 1 at $V \approx -58$ mV, where the p_a values for *Sy* and *Ki* are again at the upper and lower end of the p_a range respectively, as in Figs. 5*B* and *D*.

The listed substrate concentrations do not only confirm the $E_i(t)$ records in Figs. 3*A* and *D*, they also indicate the portion of free ions compared to the total concentrations. E.g., at 14% apoplast volume, the apoplast is very acidic, which causes a dramatic increase of free Ca^{2+} and K^+ in the apoplast compared to the situation with 9% apoplast volume. These relationships are most obvious for Ca^{2+} because it is not transported but confined to the apoplast in model *C*. From the total 18 mM Ca^{2+}, only 3 mM are free at 9% apoplast volume, whilst 15 mM are bound to the fixed anions. In contrast, at 14% apoplast volume, virtually all Ca^{2+} is free and none bound.

The calculated currents in the Table show virtual absence of K^+ currents, which reflects thermodynamic equilibrium as in the observation $E_K = V$ in Fig. 3. In contrast, Cl^- and H^+ are in a steady state: Identical values of I_{Sy} and I_{Cl} mean that substantial uptake of Cl^- through *Sy* takes place, and that Cl^- leaves the cell through *Cl* by exactly equal rates at the same time. Similarly for H^+: For a given I_{Sy}, 2 mass equivalents of H^+ enter the cell. This H^+ uptake is numerically balanced by a release through *Pu*, where I_{Pu} reflects extrusion of 1 mass equivalent of H^+. These relationships ($I_{Sy} = I_{Cl}$, and $I_{Pu} = -2I_{Sy}$) are well represented by the current data in the Table, independent of the particular volume portion of the apoplast.

Discussion

Calculations

In the initial model *A* (Gradmann et al., 1993), Eq. *4* has been used for $I_a(V)$ of all five transporters. In the version *B* of the model (Gradmann & Hoffstadt 1998), *GHK* for $I_a(V)$ of *Ko, Ki,* and *Cl,* provided the homeostatic qualities of model. Since virtually nothing is known about the effect of the substrate concentrations on the shape of *Pu* and *Sy,* the simple Ω versions of $I_a(V)$ have been chosen in model *B* for *Pu* and *Sy*. For the numerical reasons given in the Results section, the linear $I_a(V)$ for *Pu* and *Sy* have been replaced here by Eq. *6* and Eq. *7,* respectively. Whilst Eq. *6* has already been introduced in a more general form (Hansen et al., 1981), Eq. *7* is an *ad hoc* version of *GHK*. Using Eq. *7* for $I_a(V)$ of *Sy* does not mean that we assume the conditions for constant field theory to be valid for *Sy*. In particular, the condition of independent movement of ions does not make sense in case of a symporter. Nevertheless, Eq. *7* is used here, because no better approach is available. Alternatively, Eq. *8* may be used instead, if saturation kinetics $I_a(V)$ of *Sy* should be accounted for. This possibility has not been explored yet.

Ca^{2+} relations have not been forgotten in the electrical model but have been ignored because Ca^{2+} currents of mostly catalytic quantities are too small to cause significant ('stoichiometric') *V* changes directly. I.e., Ca^{2+} transport is considered to be not *V*-relevant directly and therefore is not represented in the model of electrocoupling amongst major ion transporters. However, for the buffering system in the apoplast, Ca^{2+} cannot be ignored, because there is much Ca^{2+} in the cell wall, which competes with H^+ and K^+ for association with F^-.

Oscillations

In contrast to models *A* and *B*, oscillations seem to play a minor role in model *C*. Fig. 3 provides a good example that the occurrence of oscillations in model *C* depends on rather specific parameter configurations. Under these circumstances, a detailed discussion of the characteristics of the observed oscillations (Figs. 4–6) would be rather academic. Nevertheless, these Figs. 4–6 serve as a qualitative documentation of the phenomenon. In particular, the minor effect of the surface/volume ratio on the presented oscillations of model *C* means that these oscillations of model *C* are not simple analog events to the oscillations of model *B*.

Steady State

The finding, $E_K = V$ (Fig. 3, Table), is remarkable insofar as the opposite observation, $V << E_K$ or $V > E_K$, dominates the experimental reports from plant cells and gave rise, therefore, to the suggestion that a long-term balance of $c_{K,c}$ in plant cells can only be achieved by oscillatory behavior, namely that *V* alternates in appropriate intervals between $V << E_K$ and $V > E_K$ (for review *see* Gradmann 2001). The critical point is, however, that this general observation $V << E_K$ or $V > E_K$, reflects almost exclusively the experimental conditions of model *B*, when the cells are in a bath with $c_{i,l} = const.$ This in vitro scenario, $c_{i,l} = const.$, reflects the in situ conditions of algae quite well. However, for parenchyma cells in situ this model *B* is not adequate, which was the main reason to develop model *C* in this study.

The finding, $E_K = V$, in model *C*, is noteworthy because it means that the ionic relations of parenchyma cells differ significantly from what we expect according to the current dogmata about plant cells, which are almost exclusively based on model *B* observations. $E_K = V$ in model *C*, is also obvious in retrospect, because all

K^+ pathways in the model are uniporters that obey Nernstian thermodynamics. This means that the finite amount of K^+ in model *C* will always tend to be distributed between the two compartments according to the thermodynamic equilibrium of Eq. *3*.

In contrast, the situation with H^+ and Cl^- in model *C* is not so simple. To avoid unnecessary complications, this issue is discussed here for absence of oscillations. In model *C*, Cl^- cannot reach a thermodynamic equilibrium, because the *E*'s for uptake of Cl^- through *Sy* and release of Cl^- through *Cl* are different. In consequence, there will be a steady state of zero net Cl^- translocation, in which substantial Cl^- uptake rates through *Sy* and identical rates of release through *Cl* balance each other. Analog considerations apply for H^+ translocation through *Pu* and *Sy*.

Physiological Aspects

In reality, the differences between model *B* and model *C* are probably not as sharp as emphasized so far for presentation purposes. Model *C* is still a coarse approach to real membranes, and vascular plants do not consist of parenchymatic cells exclusively.

An interesting example are the growth oscillations of pollen tubes in vitro. They strongly confirm model *B* because they precede Ca^{2+} oscillations and not the other way around (Messerli et al., 2000). Model *C* predicts absence of these oscillations in situ.

Furthermore, epidermal cells of roots can be expected to behave in an intermediate way between model *B* and *C*. On the proximal side, they face cortex parenchyma and on the distal side, the soil, which may be ion depleted also in situ but usually not in vitro. In fact, *V* oscillations of root tissue in vitro are known for a long time (Scott, 1957), and are still subject of research (e.g., Shabala & Newman, 1998). Again, according to model *C*, such oscillations should be rare in situ, i.e., in soil with limiting mineral supply.

Interestingly, guard cells in situ alternate remarkably between osmotic uptake and release. In this case, the large subsidiary cells may play the role of a virtual large apoplastic compartment, which facilitates osmotic oscillations according to our comparative investigations of model *B* and model *C*. Electrical oscillations of guard cells in vitro have been successfully described already by the initial version *A* of the electrocoupling model (Gradmann et al., 1993).

Finally, the general result, $E_K = V$, of model *C*, may be toned down when K^+ transport does not take place exclusively through uniporters, e.g., when K^+-symport becomes relevant as well (e.g., Maathuis & Sanders 1997).

This work has been supported by a grant (I/76 841) from the Volkswagen-Stiftung.

References

Amtmann, A., Klieber, H.G., Gradmann, D. 1992. Cytoplasmic Ca^{2+} in the marine alga *Acetabularia:* measurement with Ca^{2+}-selective microelectrodes and kinetic analysis. *J. Exp. Bot.* **43:**878–885

Beilby, M.J., Blatt, M.R. 1986. Simultaneous measurements of cytoplasmic K^+ concentration and the plasma membrane electrical parameters in single membrane samples of *Chara corallina. Plant Physiol.* **82:**417–422

Biskup, B., Gradmann, D., Thiel, G. 1999. Calcium release from $InsP_3$-sensitive internal stores initiates action potential in *Chara. FEBS Lett.* **453:**72–76

Blatt, M.R. 1987. Electrical characteristics of stomatal guard cells: The contribution of ATP-dependent, "electrogenic" transport revealed by current-voltage and difference-current-voltage analysis. *J. Membrane Biol.* **98:**257–274

Blatt, M.R., Beilby, M.J., Tester, M. 1990. Voltage dependence of the *Chara* proton pump revealed by current-voltage measurements during rapid metabolic blockade with cyanide. *J. Membrane Biol.* **114:**205–223

Gradmann, D. 2001. Models for oscillations in plants. *Austr. J. Plant Physiol.*, **28:**577–590

Gradmann, D., Blatt, M.R., Thiel, G. 1993. Electrocoupling of ion transporters in plants. *J. Membrane Biol.* **136:**327–332

Gradmann, D., Hoffstadt, J. 1998. Electrocoupling of ion transporters in plants: Interaction with internal ion concentrations. *J. Membrane Biol.* **166:**51–59

Hansen, U.-P., Gradmann, D., Sanders, D., Slayman, C.L. 1981. Interpretation of current-voltage relationships for "active" ion transport systems: I. Steady-state reaction-kinetic analysis of Class-I mechanisms. *J. Membrane Biol.* **63:**165–190

Maathuis, F.J.M., Sanders, D. 1997. Regulation of K^+ absorption in plant root cells by external K^+-interplay of different plasma membrane K^+ transporters. *J. Exp. Bot.* **48:**451–458

Messerli, M.A., Creton, R., Jaffee, L.F., Robinson, K.R. 2000. Periodic increases in elongation rate precede increases in cytosolic Ca^{2+} during pollen tube growth. *Dev. Biol.* **222:**84–98

Scott, B.I.H. 1957. Electrical oscillations generated by plant roots and a possible feedback mechanism responsible for them. *Austr. J. Biol. Sc.* **10:**164–179

Shabala, S.N., Newman., I.A. 1998. Osmotic sensitivity of Ca^{2+} and H^+ transporters in corn roots: effect on fluxes and their oscillations in the elongation region. *J. Membrane Biol.* **161:**45–54